Acta of Turin Polytechnic University in Tashkent, 2021, 11, 7-15
Published Online March 2021 in Acta TTPU (http://www.acta.polito.uz/)

Integrated Numerical Simulations of Gas Foil Bearing Static Performance

Ibrohim Rustamov
State Key Laboratory of Tribology, Tsinghua University, Beijing, China
Email: ibrohimru@yahoo.com

Abstract– Oil-free gas foil bearings have always been attractive in the high-speed lightly-loaded applications because of its simple and effective design. Compliance of bump foil with the interaction of top foil causes the rotor to levitate at high rotational speeds separated by air pressure. Many researches established frameworks to simplify the relationship of foil structure reaction under an unequal pressure generation along the bearing circumference. However, there is a lack of evidence to evaluate the proper model with appropriate parametric case studies. In this study, the connections between the hydrodynamic pressure in the bearing clearance and the foil assemblies are made by a coupled fluid-structure interaction (FSI) model to predict the static performance of the journal bearing. Input parameters such as eccentricity ratio and an attitude angle are applied to the initial journal position in order to capture the pressure distribution, foil deflection and load carrying capacities which were vital parameters in the performance of the rotor-bearing system. Case studies are carried out for different journal speeds and loading states to picture the bearing performance. The predicted values coincide with the published experimental data and indicate reasonable outcome.

Key words– gas foil bearing, fluid-structure interaction, computer simulations, bearing performance, eccentricity ratio, comparative study

I Introduction

Gas foil bearings (GFB) have already been centered on the researcher's attention for decades. Its preference in the high speed lightly loaded applications is due to a larger nominal film thickness for a given load, improved stability characteristics, low frictional losses, superior qualities at high temperatures and tolerance to impurities ingestion [1]. In the configuration of gas foil bearing, top foil, supported by compliant bumps underneath, wraps the journal with the aim of generating load carrying capacity during rotation thus maintains a relatively generating load carrying capacity during rotation thus maintains a relatively uniform film thickness across the hydrodynamic wedge with an air serving as a lubricant [2].

First analytical and experimental works were performed in order to evaluate the pressure development, foil attitude, load capacity, dynamic behaviors and stability of the bearing system [3, 4, 5]. The theoretical analysis of the foil journal bearings involves the integrated solution of the pressure in the radial clearance and the foil deflection by means of an iterative scheme. Further complexities are introduced by both the simplification of the structural model and fluid behavior for the gas lubricated leaf type journal bearing [6]. This type of foils can resist deflection with any combination of bending, membrane or elastic foundation effects, as the same configuration studied by Oh and Rohde [7]. In their investigation, the foil journal bearing erected from a complete shell is supported by an elastic foundation which permits the eccentricity ratios in excess of unity, as well as, both the compressible Reynolds equation and load deflection equations are coupled to perform parametric studies for a wide range of operating conditions. Braun et al. [2] develops the two-dimensional steady state and transient dynamics of a foil bearing using Navier-Stokes equations to solve the interaction between the fluid lubricant, the motion of the journal and the deformable foil boundary. Finite element method (FEM) is utilized to simulate the elastic deformation of the foil and its supports.

Integrated FE model of the foil assembly as a structural shell in combination with the hydrodynamic film defined by Reynolds equation for isoviscous ideal gas is predicted for the static and dynamic characteristics of the GFB in [8]. One-dimensional beam-like structure (1D) and flat shell (2D) models are compared for the evaluation by the results in the existing literature. The compliant bump which is modeled as a uniform elastic foundation are directly integrated in to a global stiffness matrix to relate the top foil deflections to the applied film pressure or contact pressure depending on the operating condition. The slight miscalculations are predicted for the minimum film thicknesses in the 2D model while the 1D top foil model predictions show the promising correlation between FEM and experimental results. Kim and Park [9], as well, developed a 1D analytical beam model for the

top foil deflection and implemented the Reynolds equation under both hydrostatic and hydrodynamic conditions. The sagging effect of the top foil is taken into account and experimental measurements of film thickness gives reasonable accuracy under the large loads, beyond 200 N. The decreased attitude angle is obtained with the loads increased, and vice versa for the increased speeds since a small attitude angle is a desirable feature for a stable gas foil bearing performance i.e. when the journal displacement is parallel with the load direction.

In addition to the experimental evaluations of a bearing performance, numbers of computer-based procedures are emerged to simulate the foil bearing performance calculations. For example, fluid-structure interaction (FSI) model is widely used to predict an integrated solution for the deflection of the foil structure under hydrodynamic pressure developed in the radial clearance through simultaneous and coupled iterations adopting finite element analysis (FEA) code and computational fluid dynamics (CFD) equations. This kind of two-way fully coupled FSI type is employed in [10] to obtain 3D coupled thermo-elastohydrodynamic (TEHD) solution for GFB. Thermal effects are taken into account in the gas film due to physical properties of the fluid, and bulk flow energy equation is solved by sophisticated finite difference method (FDM) code coupled iteratively to the FEA solver. Increase in the shear heating effect is attributed to the rapid growth in the temperature with the shaft speed and results agree well with the available measurements in [11].

II Model Development

1 Description of GFB

Gas foil bearings outdo conventional rigid bearings due to its operating principles of hydrodynamic lubrication and structural dynamics. The deflection of foil structures and pressure magnitude are strongly dependent on each other by the fluid-structure interaction on the inner top foil surface. Foils are welded from the one end to the bearing sleeve in the trailing edges while the leading edges remain free. Top foil covers the journal with a circumference of 355^o. Equally positioned 26 corrugated bump strips support the top foil underneath, thus making the bearing fully compliant. Foil structure material is made of a thin Inconel X-750 nickel-chromium alloy which is used for its high strength in the elevated temperatures up to 704^o. Figure 1 depicts the first generation bump type foil bearing geometry. Other given parameters of GFB in Table 1 are obtained from the experimental work of [12].

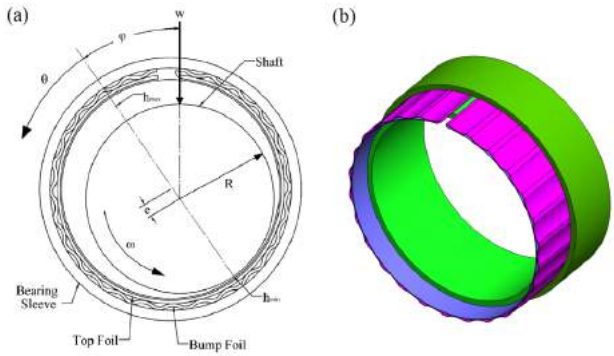

Fig. 1: Bump type gas foil bearing: a) schematics of bearing assembly, b) isometric view of 3D model

Parameters	Values
Bearing	
Radius, D=2R	38.1 mm
Length to diameter ratio	L/D=0.5, 1
Radial clearance, c	31.
Foils	
Top/Bump foil thickness, t_T, t_B	0.1016 mm
Bump length, l_B	3.556 mm
Bump pitch, S	4.572 mm
Bump height, h_B	0.508 mm
Young's modulus, E	214 GPa
Poisson's ratio, ν	0.29

Table 1: Bearing design parameters

2 Governing Equations

In the lubrication theory, coupled solution of the foil deflection and the pressure in the fluid film is needed to predict the static bearing characteristics[13]. Theoretically, the fluid motion in the radial clearance is ruled by Reynolds equation, which is an originated form of Navier-Stokes continuity and momentum equations. The equations of continuity and momentum are given, respectively:

$$\frac{d\rho}{dt} + \nabla \times (\rho \vec{v}) = 0 \tag{1}$$

$$\frac{d}{dt}(\rho \vec{v}) + \nabla \times (\rho \vec{v}\vec{v}) = -\nabla\, p + \nabla \times \tau \tag{2}$$

where, $\vec{v}$ is velocity vector, ρ is fluid density, and $p$is air pressure. External forces are neglected and the stress tensor τ is connected to the rate of strain by:

$$\tau = \mu \left(\nabla \vec{v} + (\nabla \vec{v})^T - \frac{2}{3}\delta \nabla \cdot \vec{v} \right) \tag{3}$$

In the lubrication theory, classical Reynolds equation is used frequently by ignoring inertia effects and body forces

while nullifying pressure magnitude in the film thickness direction. Assuming that no slip exists at the fluid-solid interface, an isothermal, and time invariant lubrication, the compressible Reynolds equation in Cartesian coordinates can be given as:

$$\frac{\partial}{\partial x}\left(ph^3\frac{\partial p}{\partial x}\right)+\frac{\partial}{\partial z}\left(ph^3\frac{\partial p}{\partial z}\right)=6\mu\omega R\frac{\partial(ph)}{\partial x} \quad (4)$$

where h is film thickness, μ is dynamic viscosity. In most cases, a numerical solution is needed while the Navier-Stokes equations are resolved with the CFD codes and the Reynolds equations are mostly obtained by purpose-developed codes.

If the journal is concentric relative to the bearing ($e=0$), the film thickness around the journal is constant and the bearing doesn't have any load-carrying capacity. At higher eccentricity ratios the pressure is generated and film thickness varies along the circumference. Thus the variation of film thickness depends on the eccentricity and foil deflection under the hydrodynamic pressure. The film thickness is given in the following equation:

$$h=c+e\cos(\theta-\varphi)+w_D \quad (5)$$

where

$$w_D=K_B(p-p_0) \quad (6)$$

The ratio of eccentricity is described as the ratio of eccentricity to the bearing clearance: $=e/c$. The elastic deflection of the foil structure under the exerted film pressure is given as w_D, and ϕ is recognized as an attitude angle. As mentioned, the bump foil structure behaves as an elastic backing under the top foil which provides resistance, and K_B signifies the compliance or the structural rigidity of the bump foil, which is defined as:

$$K_B=\frac{2S}{E}\left(\frac{l}{t_B}\right)^3\left(1-\nu^2\right) \quad (7)$$

where, S is pitch of bump, l is a half-length of bump, t_B is thickness of bump foil. Elastic modulus and Poisson's ratio of the foil material are given as E and ν, respectively. Consequently, the static tate of film thickness is described as:

$$h=c(1+\varepsilon\cos\theta)+K_B(p-p_0) \quad (8)$$

The resulting load components from the film pressure development parallel and perpendicular to the crossing line of bearing-journal centers are obtained by pressure integration across the bearing surface and can be formulated as:

$$W_x=2\int_0^{\pi\int}\int_0^{L/D\int} pR\sin\theta d\theta dz \quad (9)$$

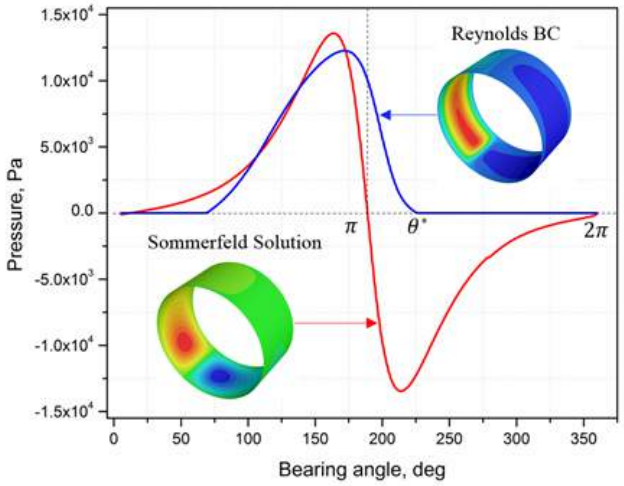

Fig. 2: Pressure distribution in a journal bearing for full Sommerfeld solution and Reynolds boundary condition.

$$W_y=-2\int_0^{\pi\int}\int_0^{L/D\int} pR\cos\theta d\theta dz \quad (10)$$

Subsequently, the total load-carrying capacity is generated by:

$$W=\left(W_x^2+W_y^2\right)^{1/2} \quad (11)$$

It should be noted that the ratios of load are the functions of L/D, and eccentricity ratios, i.e. in the $L/D>2$ ratios, predictions overestimate the load capacity for all , while the short-length-bearing theory provides more precise estimations for finite bearings of $L/D<2$, leading to excessive load-carrying capacities at small length-to-diameter ratios [14].

In the rigid journal bearings the pressure distribution can be solved by introducing the new variable which is known as a Summerfeld variable. This technique can evaluate the pressure, but the expression is not much useful, since it is hard to obtain the load components from a further integration. These difficulties are overcome by using the substitution as below:

$$1+\varepsilon\cos\theta=\frac{1-\varepsilon^2}{1-\varepsilon\cos\gamma} \quad (12)$$

Utilizing Sommerfeld replacement, the periodic boundary condition with $p=p_0$ at $\theta=0$ and 2π yields as:

$$p-p_0=6\mu\omega\left(\frac{R}{c}\right)^2\frac{\varepsilon\sin\theta(2+\varepsilon\cos\theta)}{(2+\varepsilon^2)(1+\varepsilon\cos\theta)^2}=6\mu\omega\left(\frac{R}{c}\right)^2\overline{p} \quad (13)$$

and

$$h_m = \frac{2c\left(1+\varepsilon^2\right)}{2+\varepsilon^2} \tag{14}$$

here p_0 is pressure at the point of maximum film thickness and $\overline{p}$ is dimensionless pressure. h_m is film thickness at the time of $d_p/d_x = 0$, consistent to the extreme pressure position.

According to full Sommerfeld solution, the positive pressure is generated inside the convergent film $0 \le \theta \le \pi$, and negative pressure inside the divergent film $\pi \le \theta \le 2\pi$, having the shape of skewed symmetrical pressure profile as in Figure 2. These sub-ambient pressures by the normal Sommerfeld analysis are hardly met in the actual bearings and leads to the proposal that the sub-ambient pressure calculated by the analysis have to be neglected [15]. However, the top foil is laid on the elastic foundation with no bonding, so it can separate from the bump foil to prevent the generation of subambient pressure. Therefore, in the Reynolds boundary condition the film pressure cannot be lower than the ambient pressure (p_a), and the subambient pressure is equated to zero without violating the continuity of mass flow at the outlet end. Hence, the appropriate boundary conditions for Eq. (4) are:

$$p = \frac{dp}{dx} = 0 \quad at \quad \theta = \theta^*, \quad \pi < \theta^* \le 2\pi \tag{15}$$

where the value of θ indicates the angular bearing position from the point of extreme film thickness and θ^* is the angle where $p = 0$ and $dp/dx = 0$.

3 Numerical Procedure

Analysis with the presence of fully coupled solution fields in fluid and solid domains is the nature of gas foil bearing type applications to investigate the bearing characteristics. As for the whole bearing assembly, the solution can be obtained by substituting FEM model, i.e. top and bump foil structure and CFD model, i.e. fluid film behavior. On account of the two-way interaction between the two analyses, the analyses are looped through repeatedly until overall equilibrium is reached between the structural and CFD solutions (Fig. 3). This sort of analysis is a consecutive pressure-stress analysis where nodal pressure from the fluid analysis is imported as *"fluid load"* in the succeeding stress analysis. The analysis of physical behavior is based on a sole finite element mesh along the physics. The general process is to allow in the first calculated physics file and resolve. Afterwards, reading in the next physics domain, postulate the loads to be transmitted, and resolve the following physics. The governing finite element matrix equations for the steady state simulations of the journal-fluid-foil interactions are:

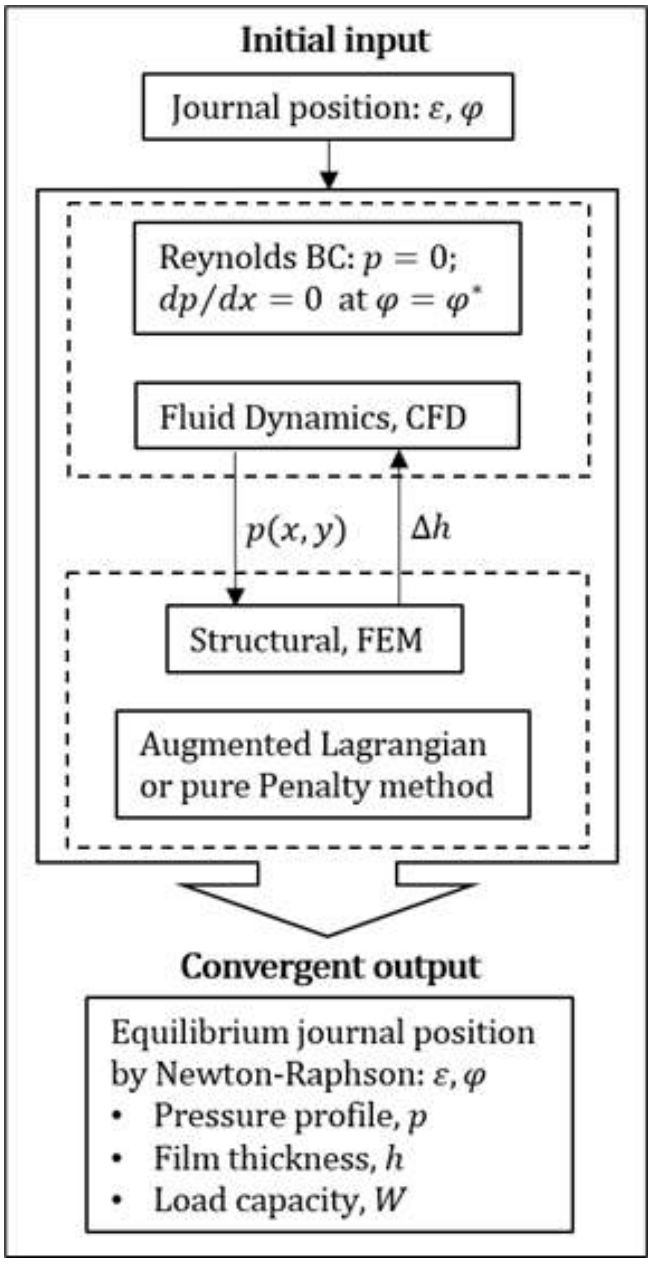

Fig. 3: Flowchart for the two-way FSI analysis process.

$$[M_S]\left\{\ddot{U}\right\} + [K_S]\{U\} = \{F_S\} + [R]\{P\} \tag{16}$$

$$\left[M_f\right]\left\{\ddot{P}\right\} + \left[K_f\right]\{P\} = \left\{F_f\right\} - \rho_0\,[R]^T\left\{\ddot{U}\right\} \tag{17}$$

Here $[M_s]$ and $\left[M_f\right]$ are the structural and fluid flow mass matrixes, $\{F_s\}$ and $\left\{F_f\right\}$ are structural and fluid force vectors, respectively. [R] represents the integrating matrix in the

actual surface area corresponding to the knots on the fluid-structure interface. Load quantities of both solid and fluid domains which are developed in that FSI interface are products of unidentified nodal degrees of freedom. Combining these indefinite loads with Eq. (16-17) produces the following:

$$\begin{bmatrix} M_S & 0 \\ \rho_0 R^T & M_f \end{bmatrix} \begin{Bmatrix} \ddot{U} \\ \ddot{P} \end{Bmatrix} + \begin{bmatrix} K_S & -R \\ 0 & K_f \end{bmatrix} \begin{Bmatrix} U \\ P \end{Bmatrix} = \begin{Bmatrix} F_S \\ F_f \end{Bmatrix} \quad (18)$$

Two-way fluid-structure interaction analysis is conducted using load transfer technique which is accessible in the ANSYS Multi-field solver environment. 3D modeling of the fluid analysis is developed in FLUENT 17.1 using pressure-velocity coupling scheme SIMPLEC with the second order pressure discretization. Pressure-based Navier-Stokes solution algorithm is enabled with the absolute velocity formulation. The boundary conditions are applied with the running pressure fixed at 101325 Pa by default. The journal surface is modeled as a moving wall against the stationary foil surface while the two edges of the bearing are defined as a pressure outlet with the measure of zero Pascal. A structured mesh with total number of nodes 3.96×10^5 is used for both fluid and solid domains. Initial parameters to start hydrodynamic process in the film thickness are taken by guessing eccentricity ratio and attitude angle and extracted loads are mapped to the structural domain. Pressure generations, film thicknesses and load-carrying capacities of the bearing are studied in different loading conditions and working operations.

At the first step of the procedure the foil surface is concentric with journal without any deflection. Assuming the initial journal position and consequential boundary conditions, the film pressures are calculated. Based on the resulting forces from pressure integration, static structural solver obtains the foil deformation which leads to a new film thickness. During the deflection of top foil, the journal travels towards the direction of the maximum deformed area, thus, the total change in the film thickness is examined by modifying the eccentricity and the attitude angle. This procedure uses Newton-Raphson iterative method to achieve convergence. Interacting structural contact models are assumed to be bonded. The augmented Lagrangian method is employed to model the contacting surfaces between foils and sleeve. This technique includes an iterative sequence of the penalty approaches which constrains the bump strips not to penetrate the top foil structure. The ultimate penetration is lower than the acceptable tolerance since the frictional stresses and contact pressure are rising during the steady-state iterations. Augmented Lagrangian technique typically results in an enhanced conditioning, and is less subtle to the amount of contact stiffness. Yet, in some studies, this method may necessitate further iterations, particularly if the distorted mesh converts into inaccurate situation.

III Results and Discussion

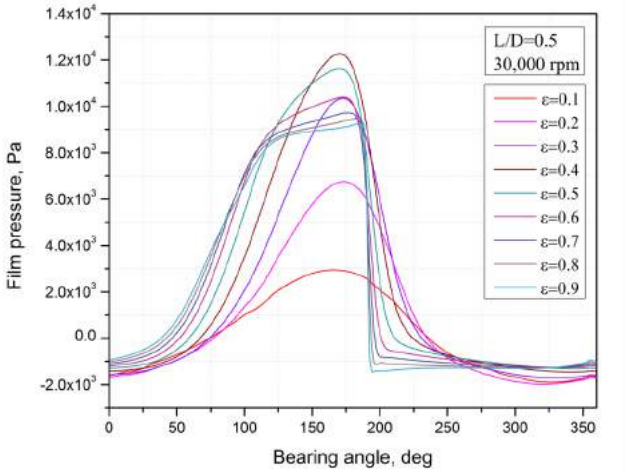

Fig. 4: Pressure distribution profiles in the bearing circumference angle for various journal eccentricities.

In this section, results are obtained for 3D fully coupled FSI model in the various bearing geometries $L/D = 0.5, 1$ and speeds at 30,000 rpm, 45,000 rpm. A structured mesh with total number of nodes 3.96×10^5 is used for both fluid and solid domains. Initial parameters to start hydrodynamic process in the film thickness are taken by guessing eccentricity ratio and attitude angle and extracted loads are mapped to the structural domain. Pressure generations, film thicknesses and load-carrying capacities of the bearing are studied in different loading conditions (up to 200 N) and working operations. The validation of the simulations is carried out to certify the reliability of the numerical codes by examining with the published experimental data in [12]. It is observed that the results are in good agreement with the experimental data with slight differences due to the simplifications in the computational process.

1 Hydrodynamic pressure and film thickness

The prediction of the film pressure generation is helpful to comprehend the bearing characteristics well. The optimum contour of the film wedge is one of the factors that results in high load-carrying capacity. Figure 4 shows the film pressure distribution on the top foil surface in the bearing speed of 30, 000 rpm for different eccentricity ratios. Obviously, in the small values of the journal eccentricity, pressure is spread uniformly both in the convergent and divergent regions of the gas film with the peak. When the value of ε exceeds 0.4,

more uniformly distributed pressure is generated only in the convergence film inlet of the bearing surface, thus the peak of the pressure is widened constantly till the outlet end where $p \geq p_0$. This process leads to a higher load-carrying capacity and beneficial in terms of the operational stability since increasing the eccentricity ratio tends to improve the convergence of the gap, or the so-called "lobbing effect" which is known to endorse greater stability at high operating speeds [16]. Hence, the load-carrying capacity is strongly dependent on the journal eccentricity since more loads can be borne in the higher values of the eccentricity ratio.

As mentioned by Hamrock et al. [14] the load ratios are strongly related to L/D and journal speed. It can be noticed in Figure 5 that in the $L/D > 2$ ratios, predictions underestimate the pressure loads as speed increases, while the short-length-bearing $(L/D < 2)$ provides higher pressure loads at small length-to-diameter ratios. Increase in the load-bearing capacity at $L/D < 2$ bearing can be attributed to the higher load concentration on the narrower foil bearing surface, as a consequence the foil deflection also becoming in a higher magnitude as the journal speed increases. Conversely, as the foil bearing surface is wider $(L/D1)$ along the axial direction, the pressure profile generated by the journal speed is dispersed on a wider foil surface, thus the pressure magnitude is lower in comparison to the narrower bearing length ratio.

In Figure 6, the values of film pressure and foil deformations are given for the journal speeds of 30,000 rpm and 45,000 rpm. Note that these values are obtained in the first step of the analysis with no load assuming on the bearing surface. Thus, the deformation of the top foil is not significant in this case. Contours of pressures with the resulting top foil deformations are illustrated in Figure 7a for =0.1 and Figure7b for =0.9 under the journal speed of 30,000 rpm. Top foil deflections are corresponded to the hydrodynamic pressure along the bearing circumference. When the journal is slightly moved toward the top foil, equally spaced "wave-like" deformations appear along the bearing circumference. While the surface of the journal approaches to the top foil surface, more concentrated waviness of deformations is experienced on the top foil surface in the direction of the bearing centerline. This shape of waviness is due to the sagging effects between the adjacent bump foil strips [5].

As shown in Figure 8, the evaluation in the minimum film thickness is made for various bearing geometries i.e. $L/D = 0.5$ and $L/D = 1$ with the same experimental data in the reference [12]. In this case, the applied loads are ranged from 5 N to 200 N according to the bearing length-to-diameter ratio (80 N for $L/D = 0.5$ and 200 N for $L/D = 1$) at various speed conditions. Both predictions and test data corresponds to the minimum film thicknesses where the maximum film pressure occurs at the bearing centerline. The smallest film thickness of 4 μm is reported in this experiment. In Figure 8a, numerical results slightly overestimate the film thickness in both cases, especially at the lighter static loads, yet the values gradually match with the obtained test points when more loads are applied. It is clear that at higher bearing speeds, the journal eccentricity adjusts itself until the load is balanced by the pressure generated in the converging gas film, forming relatively higher film thicknesses. In Figure 8b, the numerical and experimental results were very close to each other rather than the L/D ratio with 0.5. Resulted minimum film thickness was still just below 5 μm in this case too at the maximum loads. The rate of distinction between the numerical and experimental results in two L/D bearing

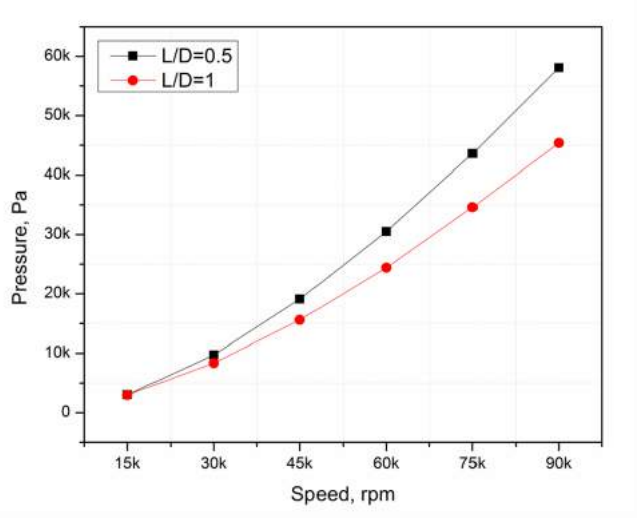

Fig. 5: Pressure loads as a function of speed for different L/D ratios

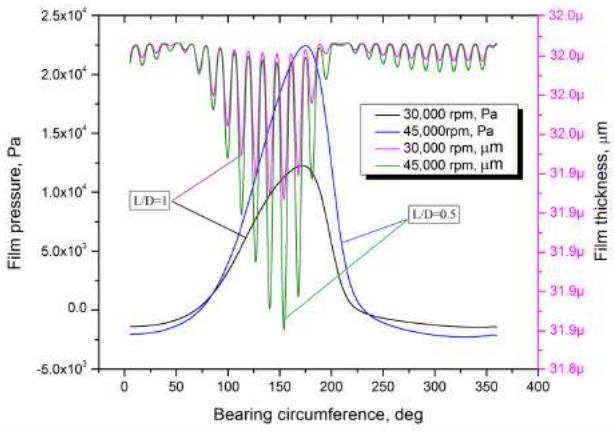

Fig. 6: Film pressure and resulting film thickness for to bearing geometry at =0.4

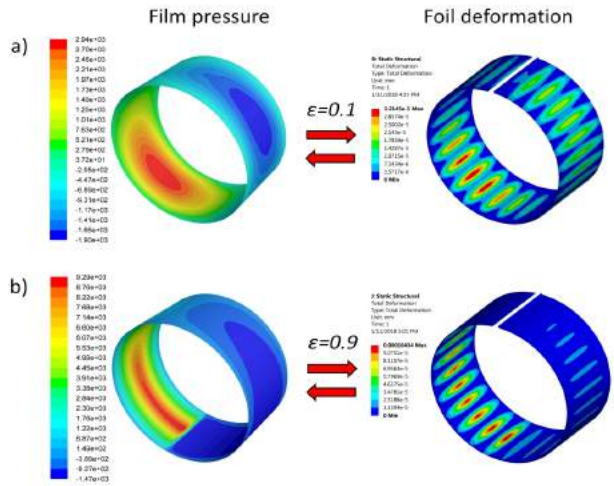

Fig. 7: Contour of pressures and corresponding top foil deformations. L/D=0.5

length to diameter ratios can be accounted for the foil bearing surface area: as the surface area increase the numerical calculations become closer to the experimental values. However, more sophisticated assumptions should be employed to precisely certify the model against the experimental values.

2 *Load-carrying capacity and attitude angle*

Numerically obtained load-carrying capacity of the bearing model is verified with the results of theory in [17] and with the experimental data reported in [18] for the first generation of foil bearings. Load-carrying capacity as a function of bearing speed is given in Figure 9. Bearing parameters and operating conditions are same for the current model. Evidently, the predicted load-carrying capacity curve is in good agreement with both theoretical and experimental results over a wide range of speeds.

According to the experiments in the work of Strom [18], the load-carrying capacity is established by gradually increasing the static load at a fixed speed and the values are noted just before the bearing seizure occurs. As for the limited resources, this type of experimental procedure can be replicated numerically by adjusting the eccentricity ratio at the highest values, still maintaining the minimum clearance between journal and foil surface. Maximum top foil deformation is used for the eccentricity modifications and the change in the attitude angle is also considered in the calculations. Pressure convergence which is based on an assumed value of ε should satisfy the enforced load through the iteration loop at a fixed operating speed until the load is converged. At the other extreme, at heavy loads the journal is forced downward and the limiting position is reached when $h_{min} = 0$ and $= c$, i.e. the journal is touching the bearing.

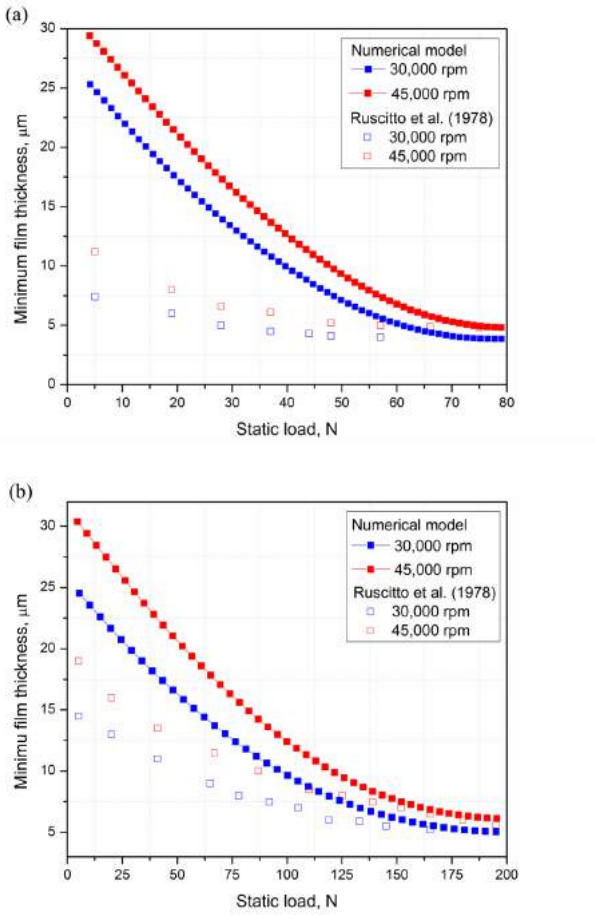

Fig. 8: Minimum film thickness versus static load: (a) L/D=0.5, (b) L/D=1. Comparison with the experimental work by Ref. [12]

One of the influencing factors in the bearing performance is an attitude angle. Small attitude angle can result in the better bearing stability. At the high speed and greater load conditions, a noticeable film thickness convergence with a small attitude angle is prone to enhance the elastohydrodynamic features in the point of whirl instability. This explains why foil bearings are able to operate at high speeds with less stability problems [19]. In the Figure 10 the journal attitude angles versus applied static loads are compared against the experimental data in [12] at the journal speeds of 30,000 rpm and 45,000 rpm. In general, numerical predictions of 3D model show good agreement with the test data in spite of the minor discrepancies at the higher bearing speed, but catching up with the test data above 140 N.

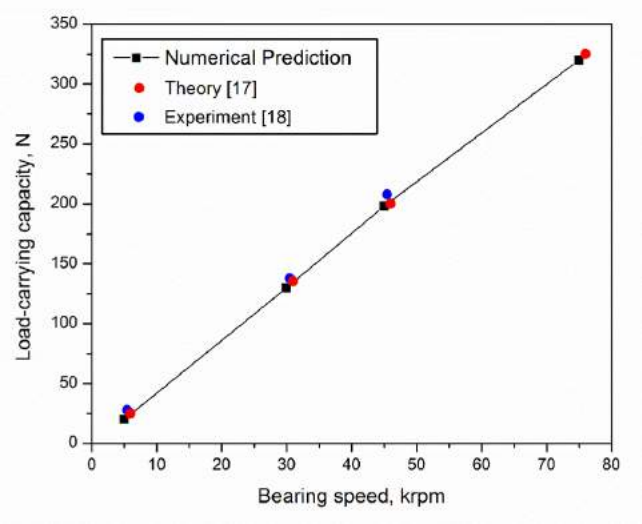

Fig. 9: Load capacity of the bearing compared with theoretical work and test data. L/D=1

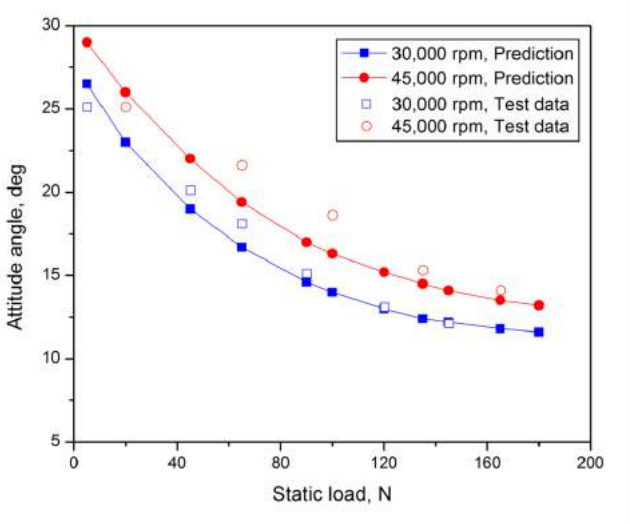

Fig. 10: Journal attitude angle versus static load. Test data is obtained from [12]. L/D=1

IV Conclusion

In this analysis, a fully coupled model of the gas foil bearing is developed by utilizing sophisticated FSI technique for the foil deflection under the hydrodynamic pressure in the film gap through the iterative solving method for the Reynolds equation and structural deformation. Commercial FEA code is employed to accomplish the whole numerical procedure with the load transfer capability. The steady-state analysis is conducted for the different parametric cases accounting for the film pressure distributions, film thicknesses, load-carrying capacity and an attitude angle. All obtained numerical results are verified by examining with the existing experimental publications and show good agreement with the test points.

From the results, it can be clearly observed that the film pressure and load-carrying capacity of the bearing is influenced by the eccentricity ratio, angular velocity and L/D ratio of the bearing. Greater load-carrying capacity is due to the higher values of the eccentricity ratio at the higher speeds. The minimum film thickness hmin5 μm is maintained despite of increase in the applied load up to 200 N. As the load and speed increased the film thickness is increased with the relatively small attitude angle. This can be attributed to the foil compliance which can adjust the clearance under the heavy loaded operational conditions. Additionally, the bump foil stiffness enhances the load-carrying capacity i.e. the energy dissipation occurs where the contacting foil surfaces have small amplitudes relative to each other. This type of analysis is concerned with the dynamic properties of the gas foil bearing accounting for Coulomb‘s law which is not considered in this work.

V Acknowledgement

The author would like to acknowledge the research support from China Scholarship Council (CSC), and funding from the Aeronautical Science Fund of China (Grant No. 20164058002) and Tsinghua University Initiative Scientific Research Program.

References

[1] H Heshmat, JA Walowit, and O Pinkus. Analysis of gas-lubricated foil journal bearings. 1983.

[2] Minel J Braun, Fred K Choy, MILORAD Dzodzo, and J Hsu. Two-dimensional dynamic simulation of a continuous foil bearing. *Tribology international*, 29(1):61–68, 1996.

[3] A Eshel and M Wildmann. Dynamic behavior of a foil in the presence of a lubricating film. 1968.

[4] H Heshmat, W Shapiro, and S Gray. Development of foil journal bearings for high load capacity and high speed whirl stability. 1982.

[5] HOOSHANG HESHMAT. Analysis of compliant foil bearings with spatially variable stiffness. In *27th Joint Propulsion Conference*, page 2102, 1991.

[6] M Carpino and J-P Peng. Theoretical performance of foil journal bearings. In *27th Joint propulsion conference*, page 2105, 1991.

[7] Kong Ping Oh and Steve M Rohde. A theoretical analysis of a compliant shell air bearing. 1977.

[8] Luis San Andrés and Tae Ho Kim. Analysis of gas foil bearings integrating fe top foil models. *Tribology International*, 42(1):111–120, 2009.

[9] Daejong Kim and Soongook Park. Hydrostatic air foil bearings: Analytical and experimental investigation. *Tribology International*, 42(3):413–425, 2009.

[10] Serdar Aksoy and Mahmut F Aksit. A fully coupled 3d thermo-elastohydrodynamics model for a bump-type compliant foil journal bearing. *Tribology International*, 82:110–122, 2015.

[11] Kevin Radil and Michelle Zeszotek. An experimental investigation into the temperature profile of a compliant foil air bearing. *Tribology transactions*, 47(4):470–479, 2004.

[12] David Ruscitto, J McCormick, Stanley Gray, and Bharat Bhushan. *Hydrodynamic air lubricated compliant surface bearing for an automotive gas turbine engine*, volume 2. Department of Energy, Office of Conservation and Solar Applications . . . , 1978.

[13] M Carpino and J-P Peng. Theoretical performance of foil journal bearings. In *27th Joint propulsion conference*, page 2105, 1991.

[14] M Carpino and J-P Peng. Theoretical performance of foil journal bearings. In *27th Joint propulsion conference*, page 2105, 1991.

[15] Bharat Bhushan. *Introduction to tribology*. John Wiley & Sons, 2013.

[16] H Heshmat. Advancements in the performance of aerodynamic foil journal bearings: high speed and load capability. 1994.

[17] Z-C Peng and MM Khonsari. Hydrodynamic analysis of compliant foil bearings with compressible air flow. *J. Trib.*, 126(3):542–546, 2004.

[18] Strom T. *Advanced Gas Turbine (AGT) Technology Development Project: Final Report. NASA CR-180891*. 1988.

[19] Christopher DellaCorte and Mark J Valco. Load capacity estimation of foil air journal bearings for oil-free turbomachinery applications. *Tribology Transactions*, 43(4):795–801, 2000.